Spill-Point Analysis and Structural Trapping Capacity in Saline Aquifers using MRST-co2lab

Halvor Møll Nilsen, Knut-Andreas Lie, Olav Møyner, Odd Andersen

SINTEF ICT, Department of Applied Mathematics, P.O. Box 124 Blindern, N–0314 Oslo, Norway

Abstract

Geological carbon storage represents a substantial challenge for the subsurface geosciences. Knowledge of the subsurface can be captured in a quantitative form using computational methods developed within petroleum production. However, to provide good estimates of the likely outcomes over thousands of years, traditional 3D simulation methods should be combined with other techniques developed specifically to study large-scale, long-term migration problems, e.g., in basin modeling. A number of such methods have been developed as a separate module in the open-source Matlab Reservoir Simulation Toolbox (MRST).

In this paper, we present a set of tools provided by this module, consisting of geometrical and percolation type methods for computing structural traps and spill paths below a sealing caprock. Using concepts from water management, these tools can be applied on large-scale aquifer models to quickly estimate potential for structural trapping, determine spill paths from potential injection points, suggest optimal injection locations, etc. We demonstrate this by a series of examples applied on publicly available datasets. The corresponding source code is provided along with the examples.

Keywords: CO2 storage, structural traps, spill-point analysis

1. Introduction

Geo-storage of CO_2 has been proposed as a possible strategy for mitigating global climate change. Under this approach, CO_2 is injected underground into deep saline aquifers, deep unmineable coal seams, depleted petroleum reservoirs, etc. [1]. Determining the maximum amount of CO_2 that can be injected and securely contained is a key question.

When injected into a water-bearing formation, density differences will drive CO_2 to form a separate mobile phase (the CO_2 plume), which is driven upwards by buoyancy. To prevent CO_2 from moving directly upward, it is injected into a permeable formation bounded upwards by a sealing caprock. Below this seal, CO_2 will spread out and slowly migrate in the upslope direction. Disregarding other trapping mechanisms, this migration continues until the plume encounters a trap in the top surface where CO_2 will accumulate. Once a trap is filled, excess CO_2 will spill over and keep migrating upwards to the next trap, and so on until the top of the formation is reached.

In the short term, structural and stratigraphic trapping are key mechanisms for geological storage of CO_2. Other important mechanisms include residual, dissolution, and mineral trapping. As CO_2 migrates upward within the rock formation, the tail of the plume will gradually withdraw, and the pore space will fill again with resident brine when CO_2 injection has stopped. However, some CO_2 will remain trapped as immobile droplets in the void space between rock grains by capillary pressure from the water. This is known as residual trapping. Over time, injected CO_2 will also dissolve in the brine, which is referred to as solubility trapping. The dissolved CO_2 will form carbonic acid that might react with the reservoir rock to precipitate carbonate minerals, leading to mineral trapping.

Herein, our primary concern is to develop methods that can quickly compute bounds on the overall capacity for structural trapping and suggest good positions for placing injection points. These methods have later been combined with simulation tools based on an assumption of vertical equilibrium [2, 3] to provide a comprehensive toolbox for optimizing injection strategies and simulating large-scale containment in a thousand-year perspective [4, 5, 6].

Structural traps correspond to local maxima of the top surface. First-order estimates of the corresponding trapping can be determined using relatively simple geometrical/topological algorithms that compute traps and catchment areas for the top surface of a given grid model. Simple percolation methods can be used to estimate spill paths, assuming that CO_2 is injected at an infinitesimal rate. These methods are implemented as free and open-source software in the Matlab Reservoir Simulation Toolbox (MRST) [7, 8]. The MRST-co2lab module [9] includes a graphical user interface for interactively exploring structural trapping, input routines for industry-standard input formats, and scripts to download, unpack and process publicly available datasets. [10, 11, 12]. Altogether, MRST provides a good platform for supporting reproducible research, which we demonstrate herein by providing provide complete scripts for all examples.

Email addresses: Halvor.M.Nilsen@sintef.no (Halvor Møll Nilsen), Knut-Andreas.Lie@sintef.no (Knut-Andreas Lie), Olav.Moyner@sintef.no (Olav Møyner), Odd.Andersen@sintef.no (Odd Andersen)

2. The spill-point approach to trap analysis

We use the term *spill path* to refer to the path followed by CO_2 below the caprock on its buoyant migration, assuming infinitesimal flow. When a trap has been completely filled by CO_2, any additional quantity entering the trap will lead to an equivalent amount exiting. For infinitesimal quantities, the flow will follow a spill path out of the trap that either terminates in a different trap or exits the domain. As such, individual traps can be seen to be connected by spill paths, much the way lakes are connected by rivers.

In line with the convention of industry-standard reservoir descriptions, a surface is represented as a quadrangular mesh using a coordinate system whose z axis is pointing downwards. We refer to this mesh as a *top-surface grid* when derived from a 3D reservoir model. Finding all traps and spill paths for a given model can be done by examining the geometry of this mesh. Although the process is simple in principle, it is sensitive to small changes in input data. We have therefore implemented two versions of the algorithm that work on dual interpretations of the quadrangular grid. The algorithms produce similar results in most cases, but sometimes the differences are significant. Comparing different outcomes can give an initial awareness of the uncertainty of the problem for a given top surface.

We refer to the two versions of the algorithm as the *corner-based* and *cell-based* approach. Both algorithms are based on the concept of *nodes* and *neighborhoods*. In the first version, nodes correspond to grid corners, whereas in the second version they correspond to cell centroids.

2.1. The basic trapping algorithm

We explain the key concepts and the basic algorithm for the corner-based algorithm, which treats the top-surface grid as a network of nodes and edges, with flow taking place between nodes along the edges. (The cell-based algorithm is similar, but uses cell centroids as nodes). To present the algorithm, some concepts used must be explained (see Figure 1):

- the *neighborhood* of an interior node is defined as the node itself plus all nodes that are immediately connected;
- the shallowest node in a neighborhood is called a *local maximum*;
- the connection between a node and each of its surrounding neighbors defines a vector and the *upslope neighbor* of a node is the one with the steepest upward slope (if any).

The association between nodes and their upslope neighbors defines a directed tree, where infinitesimal, buoyancy-driven flow occurs along paths referred to as *spill paths*, connecting each node to its upslope neighbor. Each spill path ends up in a local maximum or at a boundary node. The *spill region* of an interior local maximum is defined as all nodes on paths leading into that maximum, see Figure 2. All nodes on paths ending at a *boundary* node are assigned to the spill region of the exterior.

A *spill edge* is an edge in the mesh connecting nodes belonging to two distinct spill regions. When CO_2 flows upwards

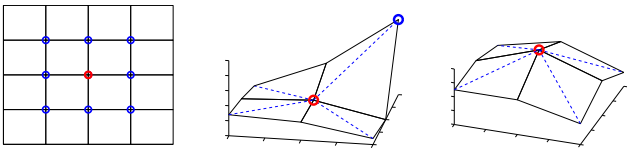

Figure 1: *Left:* the neighborhood of an internal node consists of the node itself and its surrounding nodes. *Middle:* a node and its upslope neighbor marked in blue. *Right:* a local maximum does not have any upslope node.

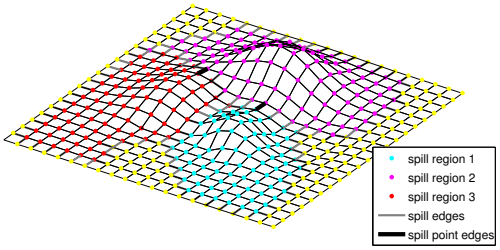

Figure 2: Three interior and one exterior spill region with associated spill edges. The spill-point edge is the shallowest spill edge connected to a spill region.

along a spill path, it will either exit the domain or accumulate near a local maximum until the surface of accumulated CO_2 reaches the shallowest spill edge of the associated spill region. This shallowest edge is called the *spill point edge*, the deepest of its two nodes called the *spill point*, and the corresponding depth is called the *spill depth*. (In degenerate cases, the spill point might not be unique). The pocket under the surface where CO_2 builds up before reaching the spill point is referred to as the *trap* associated with the local maximum. The mesh nodes within this trap are called *trap nodes* and define the *trap region* associated with this local maximum. The remaining part of the spill region is referred to as the *catchment area*.

Once the accumulated CO_2 reaches the spill point, it will start spilling out into a different spill region and follow the encountered spill path upwards. If this path ends up in a new local maximum, the trap from which CO_2 spilled out is said to be *upslope connected* to the trap associated with the new local maximum and the spill path is referred to as a *connection* or a *river*. The ensemble of traps and rivers form a directed graph. Traps associated with distinctly different local maxima may be upslope connected with each other, leading to cycles in this graph. This happens when the local traps constitute sub-pockets within a larger global trapping structure; as illustrated in Figure 3. Any cycle in the graph can thus be replaced by a single trap created by combining the involved local maxima, see Figure 4.

When two or more local traps combine in this way to define a larger trap, we say that they constitute *lower-level traps*, or *subtraps*, of a *higher-level trap*. The volume of the higher-level trap can be considerably larger than the combined volume of the lower-level traps. The process of detecting cycles and merging traps is repeated iteratively until the graph consisting of traps and rivers becomes acyclic. A trap that cannot be fur-

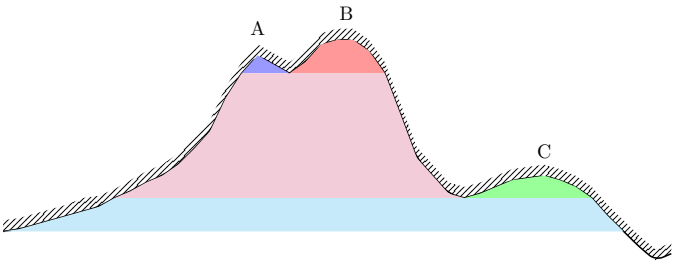

Figure 3: Illustration a trap hierarchy. *A*, *B* and *C* are local maxima with associated traps colored in blue, red and green. Trap C is upslope-connected to B, whereas A and B are upslope-connected to *each other* and are therefore subtraps of a larger trap AB shown in purple. Now, AB and C form local pockets of yet a larger trap structure ABC (cyan), whose spill point is at the far left of the domain.

ther merged is referred to as a *global trap* and is either upslope connected to another global trap or spills out of the domain.

Algorithm. Using the concepts explained above, the high-level description of the algorithm itself becomes:

1. Construct the graph $\mathcal{G}$ of individual nodes and their connections with upslope neighbors, one for each interior node that is not a local maximum. Connections to downslope neighbors are removed.
2. Assign each node to a unique spill region.
3. Identify spill edges.
4. Assign a spill-point edge to each spill region by choosing the highest of the spill edges crossing the boundary of the region.
5. Determine connections between local maxima by tracing the rivers leading from each region's spill-point edge(s) along the spill paths defined by $\mathcal{G}$. The gives a new graph $\mathcal{H}$ consisting of local maxima/traps connected by rivers.
6. Determine the global traps by iteratively removing cycles in $\mathcal{H}$ and merging the traps involved.
7. Compute the bulk volume geometrically inside each trap.

2.2. *Interface and implementation in* `MRST-co2lab`

To use the functionality in `MRST-co2lab`, the first thing one has to do is to create a semi-2D description of the top surface which includes a set of data objects that provide mapping between each cell in the 2D surface grid and a representation of the volumetric column that lie beneath in 3D. The top-surface grid can either be generated from a 3D volumetric grid using the function `topSurfaceGrid` or from a compatible set of depth and thickness maps. The common interface to the two versions of the algorithm described above is the function `trapAnalysis`. As an illustrative example of the type of information that can be obtained from this function, we consider a box geometry of $10,000 \times 5,000 \times 50$ m^3. We introduce a sinusoidal perturbation of the top and bottom surfaces, move the box to a depth of 1000 m, and assign a uniform porosity of 0.25. Figure 5 shows the 3D grid and the extracted top surface plotted on the same axes. Assuming that the surface represents an impermeable seal, the local domes will represent structural traps,

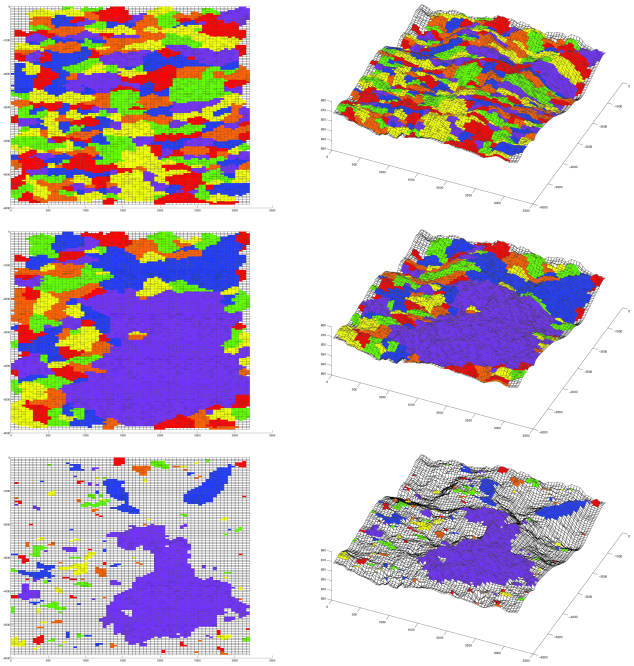

Figure 4: By merging local maxima into global traps, 335 initial spill regions (top row) are reduced to 128 global spill regions (middle row) and traps (lower row).

which we identify using the trapping algorithms. All global traps can be identified from the array that associates an integer to each cell in the top-surface grid. For cells located *within* a trap, the integer represents the index of that trap; for other cells, the integer is a zero.

Next, a percolation type analysis can establish in which direction CO_2 will migrate from each cell if injected at an infinitesimal rate. The mapping between cells and spill regions is represented by a vector, with zero components for cells spilling out of the domain. The directed graph describing connections between traps is represented using an adjacency matrix, whereas cells on spill paths between traps are stored in a cell array. In the middle plot of Figure 5, we visualize traps and connections.

In the non-degenerate case, each trap has either zero or one upslope connection. The graph of traps and connections will then consist of a set of separate trees. Each tree has a root, defined as a trap with no upslope neighbors, and a set of branches that each consists of traps connected to the root via rivers in the upslope direction. For each tree, we also define a set of leaf nodes, consisting of those traps which no other traps spill into. If any trap has more than a single upslope connection, the strict division into separate trees cannot be applied, but the concepts of roots, branches and leaf nodes remain meaningful, although a branch may now lead into more than one root node.

In Figure 5, the directed graph consists of three trees: The largest tree emerges from trap number one, forms two main branches, and contains nine global traps. The second tree emerges from trap number two and consists of three global traps forming a single branch. The third tree consists of a single root,

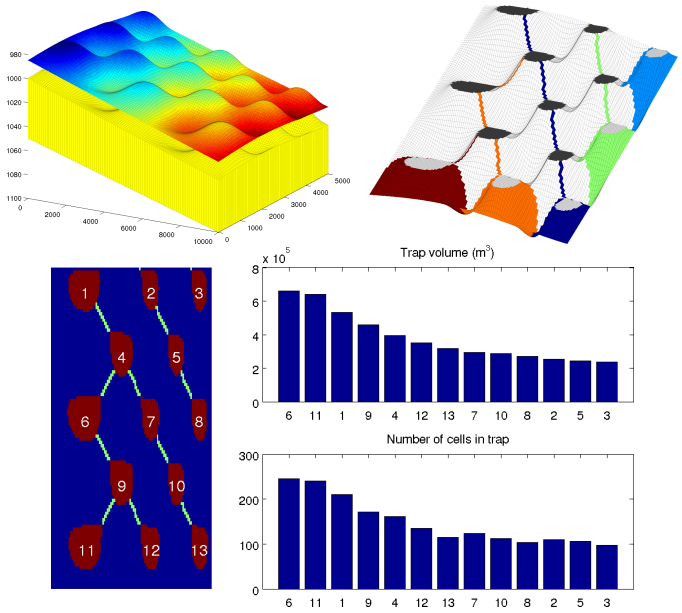

Figure 5: Conceptual model illustrating the trapping structure. *Upper left:* the extracted top-surface grid has been shifted slightly upwards and colored by depth values to clearly distinguish it from the yellow 3D grid. *Upper right:* leaf traps flattened at the spill level (light gray), the surrounding catchment areas (shown in different colors), and the spill-paths to the top of the domain; the spill levels of up-slope traps are shown in dark gray. *Lower left:* individual traps (red) and the rivers connecting them (green). *Lower right:* pore volume and the number of cells contained in each trap.

trap number three.

The total volume of a trap is limited by the top surface within the trap and the lateral plane at the spill depth. The pore volume of all traps can be computed using the function `computeTrapVolume`. For this particular model, the thirteen traps provide a combined trapping capacity amounting to 8% of the total pore volume. Bar plots of trap volumes and number of cells are shown to the right in Figure 5.

`MRST-co2lab` also contains an interactive viewer that simplifies the trapping analysis. In forward mode, the user can select a point inside any trap or catchment area to identify the migration path(s) and upslope connected traps. Individual traps can also be inspected in more detail. In backward mode, the user can determine all traps downslope from a given point. Figure 6 shows an example of using the viewer in forward mode. On the figure, cell number 1898 has been chosen as the injection point. This cell is within the catchment area of trap 11, which contains 13% of the total trap volume of the model. Further migration from here will reach traps 9, 6, 4 and 1, thereby utilizing 54% of the total trap volume. To produce the plot in Figure 6, we pass parameters to `interactiveTrapping` specifying that we want to use the cell-based method, the model should be shaded, catchment areas displayed, and traps along the spill path marked using shades of gray.

The complete setup and all statements necessary to produce Figures 5 and 6 can be found in the script `trappingExample1.m`.

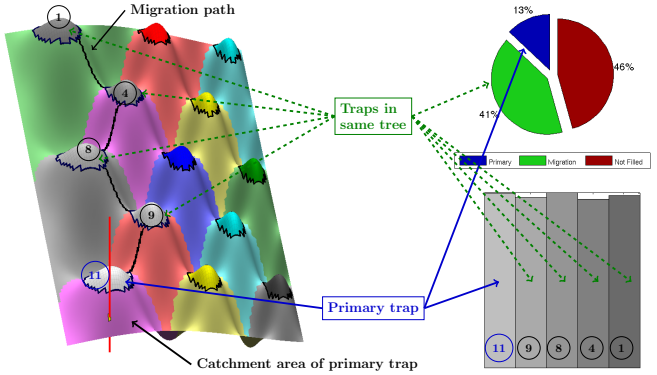

Figure 6: Interactive view in forward mode. The pie chart shows the volume of the trap whose catchment area contains the injection point ('primary'), the combined volume of traps along the associated spill path ('migration'), and the volume of all other traps ('not filled'). The bar plot displays the volume of each trap along the spill path. The scale is logarithmic, since realistic scenarios tend to have widely varying trap sizes.

3. Application to public data sets

In this section, we apply the tools described to different public data sets to estimate the potential for structural trapping. Spill paths, catchment areas, and structural traps are identified without any flow simulation, and this computation has a low cost and can be performed interactively even for large models. We therefore recommend that these simple geometrical analysis tools are used as starting points for more comprehensive simulation studies. By exploring the grid interactively one can, for instance, seek to determine the best possible injection site with regards to accessible structural trapping capacity, e.g., as discussed in detail in [4, 5, 6].

3.1. Trapping capacity for North Sea aquifers

The data sets published by the Norwegian Petroleum Directorate (NPD) as part of a recent CO_2 Storage Atlas [10] represent real aquifers from the Norwegian North Sea. These data cover large areas and are primarily meant for mapping. The extracted top-surface grids will be very coarse, but can still be used to provide indicative estimates of structural trapping capacity and likely outcomes for specific injection scenarios. In the atlas, twenty-one geological formations have been individually assessed and grouped into saline aquifers considered as candidates for CO_2 injection. To establish a volumetric grid, a depth map of the top surface and a map of the formation thickness are required. The published data include formation thicknesses and depth maps for many of the formations in Figure 7, but not all formations have both, and even when both are present, their coordinates do not always overlap. Nevertheless, using interpolation of non-matching, scattered data for the thickness maps, we were able to construct models of fourteen different sand volumes shown in Figure 8. Table 1 reports estimated bulk volumes inside structural traps. The results are not directly comparable with [10] which studies subsets or combinations of formations and incorporates petrophysical data and

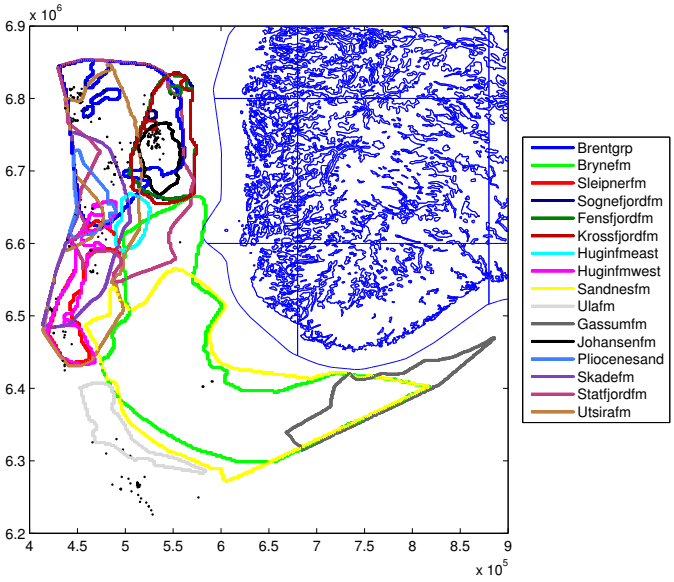

Figure 7: Geological formations in the North Sea CO_2 Storage Atlas [10]. The black dots indicate wells from the NPD's public database (`http://factpages.npd.no/factpages/`). The map of Norway comes from the Norwegian Mapping Authority (`http://www.kartverket.no/`) and is used for scale and rough positioning.

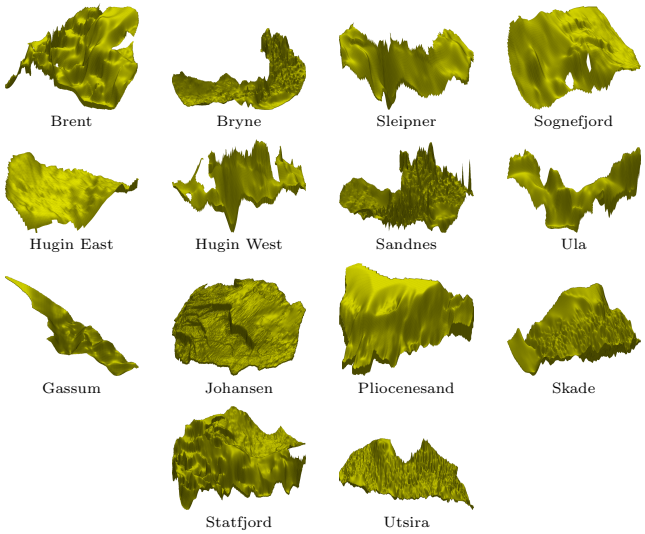

Figure 8: Reconstructed grid models for fourteen different sand volumes derived from the public data sets accompanying the CO_2 Storage Atlas of the Norwegian North Sea [10].

simulation-based adjustment factors that are not publicly available. We have chosen to present our results directly on individual formations as this gives unequivocal results that should be easy to reproduce for other researchers. In [4, 5, 6] estimates reported herein are refined to account for geophysical rock properties and density variations in CO_2 with depth for the Sandnes, Skade, and Utsira formations. We also provide back-of-an-envelope estimates of the upper bounds on residual and solubility trapping.

As can be seen from Table 1, there are large differences in the fraction of the aquifer volumes contained within structural traps. There are also significant differences in the estimates provided by the two variants of the trapping algorithms, as many of the aquifers have traps with lateral sizes close to the data resolution. The complete source code of the example is given in script `describeAtlas.m`.

Of all models in the CO_2 Storage Atlas, the Hugin West Formation has the largest relative difference in trap volumes as estimated by the corner-based and cell-based algorithms, and thus serves as a useful case to highlight the differences between them, illustrating the instabilities inherent in the geometrical algorithm for identifying small traps. Figure 9 shows that the top surface is relatively smooth and steep, with only eight identifiable structural traps. Compared with other formations, two of these are medium sized, while the remaining six are relatively small.

Because the two algorithms interpret the top-surface grid differently, they will generally assign a different number of cells and also compute different volumes for each trap. The corner-based method will tend to compute more precise spill points than the cell-based one, since cell centroids have originally been computed as grid corner averages. For trap number one,

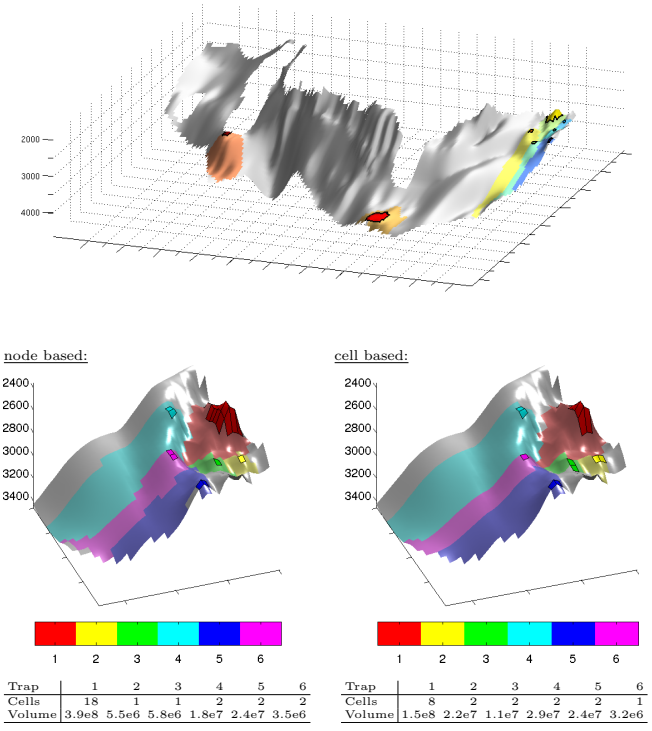

Figure 9: Structural traps for the Hugin West Formation. *Upper plot:* the whole formation with structural traps and catchment areas given in different colors. *Lower plots:* the six traps identified by the two different algorithms in the southern parts of the formation located to the right in the upper plot; volume estimates are in cubic meters. Complete script: `trapsHuginWest.m`.

Table 1: Total bulk volumes and bulk volumes inside structural traps for different formations from the CO_2 Storage Atlas [10] measured in cubic meters. Porosity and reference density must be supplied for each formation to derive estimates for CO_2 storage capacity.

		Depth		Rock	Corner-based traps		Cell-based traps	
Name	Cells	min	max	volume	volume	%	volume	%
Brentgrp	21096	1659	5569	3.41e+12	9.63e+10	2.83	9.47e+10	2.78
Brynefm	46585	271	4060	4.41e+12	3.33e+11	7.54	3.30e+11	7.48
Sleipnerfm	5116	2090	5323	2.63e+11	1.13e+09	0.43	1.07e+09	0.41
Sognefjordfm	9382	713	4145	9.06e+11	2.70e+10	2.98	2.91e+10	3.21
Huginfmeast	2264	2173	2893	9.26e+10	3.53e+08	0.38	2.89e+08	0.31
Huginfmwest	5513	1946	4617	3.75e+11	1.20e+09	0.32	8.34e+08	0.22
Sandnesfm	45126	320	3411	1.55e+12	2.13e+11	13.75	2.13e+11	13.81
Ulafm	4544	2299	4536	3.99e+11	1.53e+09	0.38	1.61e+09	0.40
Gassumfm	35043	305	3679	6.23e+11	4.78e+10	7.67	4.77e+10	7.65
Johansenfm	78630	1822	3233	3.39e+11	2.60e+10	7.68	2.61e+10	7.71
Pliocenesand	13520	260	641	2.90e+11	6.86e+07	0.02	7.15e+07	0.02
Skadefm	52531	468	1257	2.33e+12	3.86e+09	0.17	3.86e+09	0.17
Statfjordfm	122076	1636	6202	4.14e+12	9.37e+10	2.26	9.31e+10	2.25
Utsirafm	97529	318	1391	3.84e+12	1.68e+10	0.44	1.68e+10	0.44

the cell-based method computes a shallower spill depth, and significantly fewer cells are identified as part of the trap. For trap number four and five, both approaches identify the same trap cells, but trap volumes differ due to different identified spill depths.

To avoid ambiguities, the cell-based method excludes cells whose centroid depths *equal* the depth of the trap's spill point, as such cells might belong to the boundary of multiple traps and their inclusion would in any case not contribute to the trap volume. For trap number six, the corner-based method computes the spill point at 2746.6 m, slightly deeper than the centroid of the cell identified as the spill point in the cell-based algorithm. This cell is therefore assigned as part of the trap only by the corner-based approach. The 20 cm depth difference may appear small, at least compared to the vertical resolution seen in 3D models for large-scale, long-term simulations, but leads to significantly different bulk volumes of the trap (3.5 vs. 3.2 million cubic meters) when trap height is multiplied by cell areas.

The corner-based approach does not necessarily include all cells surrounding a trap node as part of the trap. The projection of traps from corners to cells will only include cells whose centroids are shallower than the spill depth. Traps 2 and 3 in the corner-based approach consist of only one cell each. The spill depths determined by the cell-based algorithm for these two traps are somewhat deeper, thereby including one additional cell in each trap and yielding significantly different trap volumes.

In their current implementations, the corner-based method considers a 9-point neighborhood stencil, whereas the cell-based uses a 5-point stencil (similar to the industry-standard two-point discretization) and hence gives spill paths that tend to follow axial directions to a higher degree. This effect is seen on the boundary of the catchment areas in Figure 9.

3.2. *Effects of data resolution: the Johansen Formation*

The Johansen Formation was previously proposed as a potential injection site in connection with the planned capture of CO_2 from the gas power plant at Mongstad. A full field model

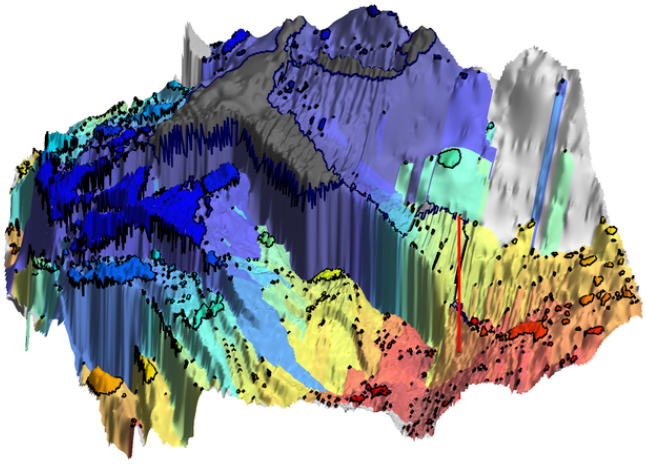

Figure 10: Potential for structural trapping from a single injection point in the Johansen Formation predicted using a model from the CO_2 Storage Atlas [10]. Dark colors signify structural traps, whereas light colors are the corresponding catchment areas. Light gray colors represent areas that spill to the perimeter of the model, whereas structural traps encountered along the spill path are shown in dark gray.

and four different sector models were developed in collaboration with NPD [13] and later made publicly available [11]. A simplified subset of one of the sector models was later used in a code comparison study [14, 15]. Herein, we will use the same injection point as studied in [13] and discuss qualitative differences in structural traps and spill-point paths computed on the full-field model, one of the sector models ('NPD5'), and on a model with higher resolution derived from data supplied with the CO_2 Storage Atlas [10]. The *quantitative* effects of using different spatial resolutions for the latter model are discussed in detail in [6]. Figure 10 shows the spill path, catchment areas, and structural traps for the atlas model, whereas Figure 11 outlines the geographic extent of the three models and contrasts the differences in spill paths, catchment areas, and structural traps for all models.

Atlas model:

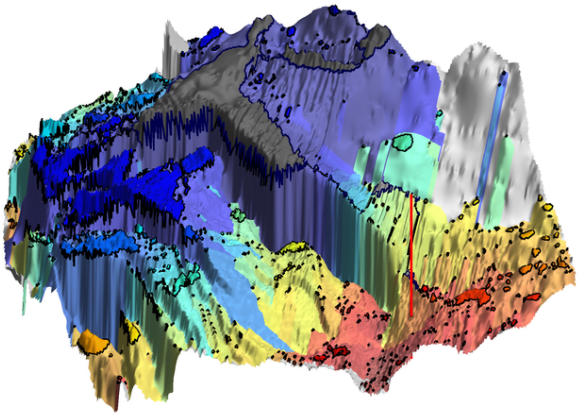

All three models:

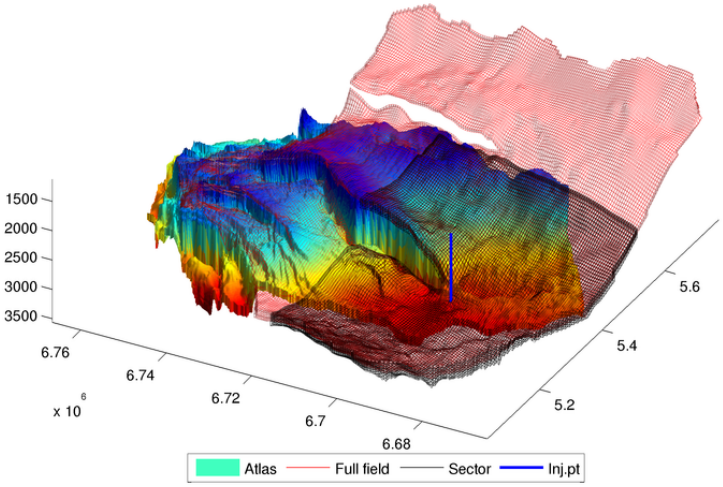

'Full-field' model:

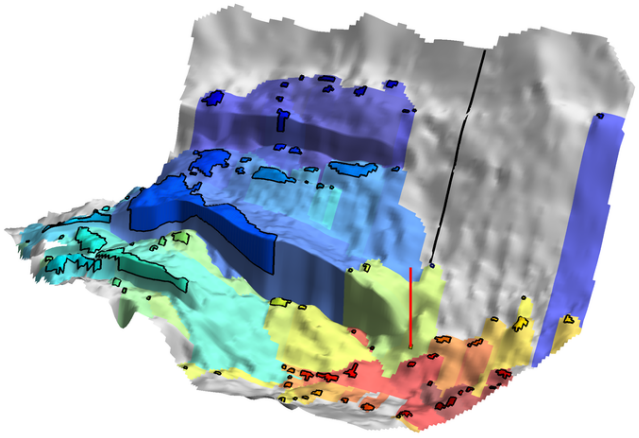

Sector model:

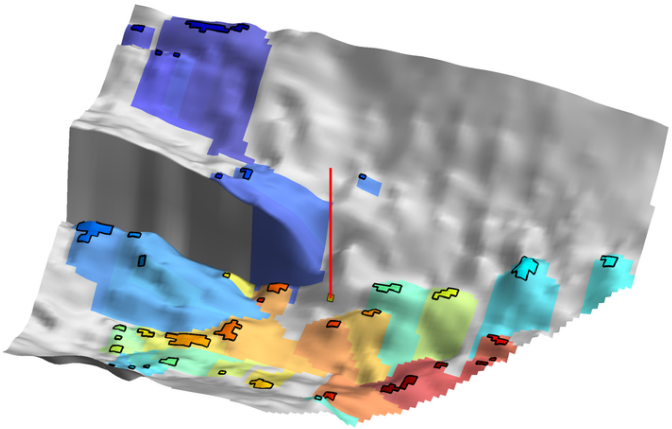

Figure 11: Structural trapping for three different models of the Johansen Formation: the model from the CO_2 Storage Atlas (upper left) and a 'full field' model (lower left) and a sector model (lower right) developed by the Norwegian Petroleum Directorate. In the upper-right plot, the three models are superposed, with the Storage Atlas model colored by surface elevation, the sector model as a black grid, and the 'full-field' model as a red grid. Structural trapping is computed using the cell-based algorithm. Complete script for this example: `trapsJohansen.m`.

The NPD models have much lower resolution than the atlas model and hence give smoother top-surfaces containing significantly fewer traps. The injection point is not located within a catchment area in the sector model. In the atlas model, the injection point is located in the accumulation area of a small trap that further connects to a series of small traps. An intricate migration path is followed that first moves up towards the blue-green area, then turns to follow the ridge at the sealing fault and finally ends in the large traps marked in dark gray color. The corresponding large trap for the 'full-field' model is shown in dark blue color, but is here not part of the migration path. Because of the lower resolution, most of the small-scale traps are not resolved, and the migration path ends up describing an almost straight line towards the crest of the model. Finally, notice that neither of the models provide information about the large fault.

3.3. Uncertainties in capacity estimates: the IGEMS data

Next, we will use a large ensemble of equiprobable top-surface realizations to illustrate the large uncertainties in capacity estimates that should be expected when working with models based on sparse data. The ensembles of synthetic aquifer models that make up the IGEMS data set [12] were originally generated to investigate how variations in the top-surface morphology with a relief amplitude below seismic resolution would influence CO_2 storage capacity [16, 17]. Each model realization describes a large 30×60 km sandbox in the shape of an inverted gutter. Fifteen different types of top-surface morphologies were designed by combining three different stratigraphic scenarios—flat deposition, buried beach ridges in a flooded marginal-marine setting (FMM), and buried offshore sand ridges (OSS)—with five different structural scenarios: no faults, uniform (UP) or random (NP) fault displacement and length, and either a single 90° strike (1) or 30° and 90° strike directions (2). Offshore sand ridges with uniform faults and a single strike direction will hence be referred to as OSS UP1, and so on. Figure 12 shows the corresponding fold and fault traps for each of the fifteen scenarios.

For each of these fifteen scenarios, one hundred different surfaces with a 100×100 m resolution were generated stochastically. Estimates of structural volumes reported in [16, 17] were obtained using an early implementation of the cell-based method discussed herein. Figure 13 compares average structural volumes computed by the corner-based and cell-based versions of the trapping algorithm. For the flat deposition there are only fault traps, and the two methods compute almost the same total volumes. Not surprisingly, the nonuniform structural cases, whose faults have 20–150 m displacement and 300–6000 m length, exhibit larger variation than the uniform cases, where faults have 100 m displacement and 4000 m length. The offshore sand ridge (OSS) cases are characterized by rather large lobes (amplitude <20 m, width 2–4 km, length 10–60 km, and spacing 2–4 km). Here, large fold traps dominate the smaller fault traps, and once again the relative deviations between the two methods are small. The flooded marginal-marine (FMM) scenarios, on the other hand, have much denser and smaller lobes (amplitude 1–10 m, width 10–300 m, length less than 15

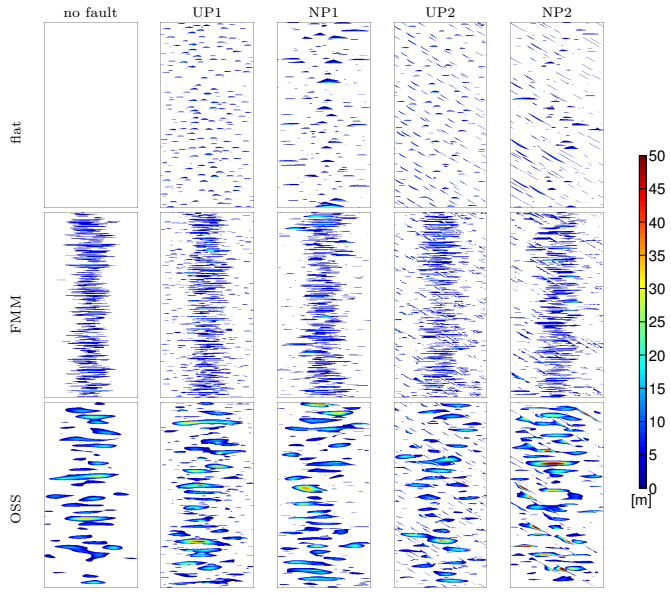

Figure 12: Height inside structural traps in meters computed by the cell-based method for one realization of each of the fifteen different structural and stratigraphic scenarios from the IGEMS project. The x-axis is the 30 km east–west axis of the aquifer, and the y-axis the 60 km north–south axis. Complete script: `showIGEMS.m`.

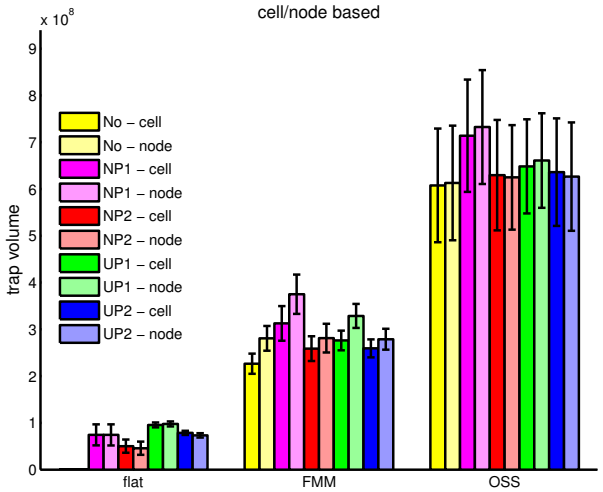

Figure 13: Average volume available for structural trapping for one hundred realizations of each of the fourteen different top-surface scenarios defined in the IGEMS project. The vertical lines show the standard deviation. The five different structural scenarios are shown in different color: 'No' refers to cases without faults, 'UP' refers to uniform fault displacement and length, 'NP' refers to random fault displacement and length, '1' refers to a single 90° strike, and '2' refers to two cases with 30° and 90° strike directions. Complete script: `trapsIGEMS.m`.

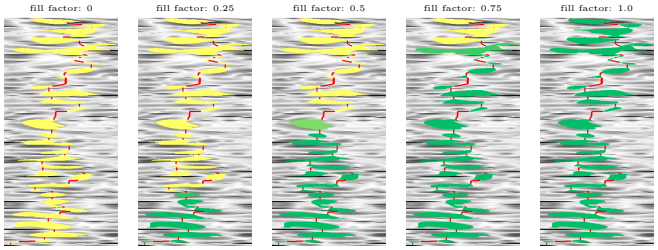

Figure 14: Gradual filling of the main branch of the trapping tree for the scenario with offshore sand ridges and nonuniform faults with a 90° strike direction ('OSSNP1'). Complete script: `fillTreeIGEMS.m`.

km, spacing 40–300 m) which result in intricate patterns of fold and fault traps that are similar in size. Because the corner-based method always chooses spill points at least as deep as those identified by the cell-based method, the computed trap volumes will also be larger. In fact, for the flat, NP1, and OP1 structural scenarios, this difference in interpretation of the top surfaces gives larger differences in the averaged volumes than the standard deviation of among the different stochastic realizations. Finally, we notice that faults normal to the up-dip direction will increase the storage capacity, in particular for the FMM cases, whereas adding a second fault system with a strike angle of 30° will open some of the fold traps and hence lead to slightly lower structural trapping capacity.

By visualizing how branches in the trapping tree gradually fills up, the percolation type analysis used above can give an idea of the dynamics of a specific injection scenario, as illustrated in Figure 14.

3.4. Finding optimal injection points: the Utsira Formation

In the final example, we demonstrate how information about structural traps and their connections can be used to guide injector placement. We consider the problem of determining where n_w wells should be placed in order to optimize the potential for structural trapping.

Assuming that the injection of CO_2 will take place at an infinitesimal rate, candidates for optimal injection points can be identified by considering the leaf nodes of the trees in the trapping structure. By identifying the n_w leaf traps that spill into the largest combined part of the trap network, and positioning the wells to spill into these, an optimal configuration is determined. The following "greedy" algorithm can be used:

1. Identify all leaf traps
2. For each leaf trap, identify the set of upslope traps and compute the combined volume (including that of the leaf trap itself).
3. Find the leaf m with the largest combined volume, and add it to the list of optimal leaf traps.
4. Set the volume of traps upslope of m to zero.
5. Repeat from Step 2 until either n_w optimal leaf traps have been determined or there are no more trees with a non-zero volume.

This strategy ensures well positions that maximize the potential for structural trapping under the assumption of infinitesimal

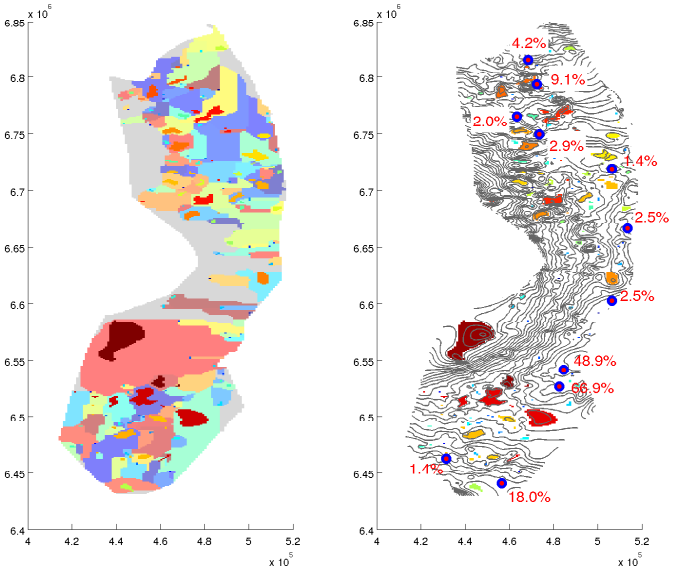

Figure 15: Identification of good injection points in the Utsira Formation. *Left:* all traps and their associated catchment areas. *Right:* traps colored by the total volume of the tree they belong to, eleven injection points, and the fraction of the total trap volume that can be reach by migration from each injection point.

flow. However, in reality the CO_2 will be injected at a finite rate and form a volumetric plume with nonzero thickness and finite extent. One might therefore also consider locating the injection points on the ridges *between* trap regions corresponding to different trees (or distinctly different branches) with similarly-sized upslope trapping volume. Injecting at these points would allow CO_2 to migrate simultaneously into different trees (or branches). Sometimes, filling two medium-size trees could be a better injection strategy than filling a single large tree, both in terms of maximizing the structurally trapped volume, and balancing pressure buildup.

In Figure 15 we have applied the strategy above on the Utsira Formation model from [10] to compute the ten largest trapping trees, along with eleven injection points representing the best locations on ridges between two trees.

For realistic scenarios, additional factors need to be considered. The injection point should not be located too close to a spill region leading out of the domain, to avoid significant leakage when injecting at a finite rate. Injectivity and local heterogeneity should also be considered. Determining optimal injection *rates* remains an important task. In a practical workflow, the strategy outlined above can be used as a preprocessing stage to efficiently identify good starting points which can subsequently be improved upon using more comprehensive methods.

4. Concluding remarks

Through our examples we have tried to illustrate the large uncertainties and the resulting differences in simulated outcomes that can be expected and should be properly accounted for in real models. The actual numbers presented for real aquifers are based on the very limited data that are publicly available and

should therefore not be taken literally as reliable estimates of actual storage capacities. However, given sufficient data, we believe that using simple tools for computing structural traps, catchment areas, and spill-point paths will be instructive as a means to rapidly investigate effects of data resolution, guide the placement of injection wells, and explore large portions of the parameter space.

We have presented two classes of algorithms for computing structural trapping and estimates of migration paths. They are geometrically dual in the sense that one considers connections between cell centers and the other relies on connections between cell corners. Both algorithms are inspired by ideas for primary migration of oil and gas, or equivalently, by concepts in water management like drainage areas and waterway networks. They have to the best of our knowledge not been used in the setting of geological CO_2 storage before. In particular, we have outlined the algorithms used, demonstrated their sensitivity to geometry variations, and demonstrated how to identify injection points with the largest potential for structural trapping. In general, we believe that much of the information needed to optimize a CO_2 injection scenario can be obtained using simplified tools that honor the main dynamics in the system, gravity flow, as also noticed by [18], who used percolation type of calculations. In [4, 5, 6], we demonstrate how the tools described herein can be combined with vertical-equilibrium models and rigorous mathematical optimization to develop scenarios for the injection of hundreds of megatonnes of CO_2 into saline aquifers in the North Sea.

All methods are implemented using the CO_2 module of the Matlab Reservoir Simulation Toolbox, and are freely available as open-source code [9]. All examples are based on open data and come with full MRST scripts.

Acknowledgments

The work was funded in part by Statoil ASA and the Research Council of Norway through grants no. 199878 (Numerical CO_2 laboratory) and 21564 (MatMoRA-II).

References

[1] S. M. Benson, et al., Underground geological storage, in: IPCC Special Report on Carbon Dioxide Capture and Storage, Intergovernmental Panel on Climate Change, Cambridge University Press, Cambridge, U.K., 2005, Ch. 5.

[2] H. M. Nilsen, K.-A. Lie, O. Andersen, Robust simulation of sharp-interface models for fast estimation of CO_2 trapping capacity, submitted.

[3] H. M. Nilsen, K.-A. Lie, O. Andersen, Fully implicit simulation of vertical-equilibrium models with hysteresis and capillary fringe, submitted.

[4] O. Andersen, H. M. Nilsen, K.-A. Lie, Reexamining CO_2 storage capacity and utilization of the Utsira Formation, in: ECMOR XIV – 14^{th} European Conference on the Mathematics of Oil Recovery, Catania, Sicily, Italy, 8-11 September 2014, EAGE, 2014. doi:10.3997/2214-4609.20141809.

[5] K.-A. Lie, H. M. Nilsen, O. Andersen, O. Møyner, A simulation workflow for large-scale CO_2 storage in the Norwegian North Sea, in: ECMOR XIV – 14^{th} European Conference on the Mathematics of Oil Recovery, Catania, Sicily, Italy, 8-11 September 2014, EAGE, 2014. doi:10.3997/2214-4609.20141877.

[6] H. M. Nilsen, K.-A. Lie, O. Andersen, Analysis of trapping capacities in the Norwegian North Sea using `mrst-co2lab`, submitted.

[7] K.-A. Lie, S. Krogstad, I. S. Ligaarden, J. R. Natvig, H. M. Nilsen, B. Skaflestad, Open source MATLAB implementation of consistent discretisations on complex grids, Comput. Geosci. 16 (2012) 297–322. doi:10.1007/s10596-011-9244-4.

[8] The MATLAB Reservoir Simulation Toolbox, version 2014a, `http://www.sintef.no/MRST/` (May 2014).

[9] SINTEF ICT, The MATLAB Reservoir Simulation Toolbox: Numerical CO_2 laboratory (Oct. 2014).
URL `http://www.sintef.no/co2lab`

[10] E. K. Halland, W. T. Johansen, F. Riis (Eds.), CO_2 Storage Atlas: Norwegian North Sea, Norwegian Petroleum Directorate, P. O. Box 600, NO–4003 Stavanger, Norway, 2011.
URL `http://www.npd.no/no/Publikasjoner/Rapporter/CO2-lagringsatl`

[11] G. Eigestad, H. Dahle, B. Hellevang, W. Johansen, K.-A. Lie, F. Riis, E. Øian, Geological and fluid data for modelling CO2 injection in the Johansen formation (2008).
URL `http://www.sintef.no/Projectweb/MatMorA/Downloads/Johansen`

[12] Norwegian Computing Center, Impact of realistic geologic models on simulation of CO_2 storage (2013).
URL `http://www.nr.no/IGEMS/`

[13] G. Eigestad, H. Dahle, B. Hellevang, F. Riis, W. Johansen, E. Øian, Geological modeling and simulation of CO2 injection in the Johansen formation, Comput. Geosci. 13 (4) (2009) 435–450. doi:10.1007/s10596-009-9153-y.

[14] H. Class, A. Ebigbo, R. Helmig, H. K. Dahle, J. M. Nordbotten, M. A. Celia, P. Audigane, M. Darcis, J. Ennis-King, Y. Fan, B. Flemisch, S. E. Gasda, M. Jin, S. Krug, D. Labregere, A. N. Beni, R. J. Pawar, A. Sbai, S. G. Thomas, L. Trenty, L. Wei, A benchmark study on problems related to CO2 storage in geologic formations, Comput. Geosci. 13 (4) (2009) 409–434. doi:10.1007/s10596-009-9146-x.

[15] L. Wei, F. Saaf, Estimate CO2 storage capacity of the Johansen formation: numerical investigations beyond the benchmarking exercise, Comput. Geosci. 13 (4) (2009) 451–467. doi:10.1007/s10596-008-9122-x.

[16] H. M. Nilsen, A. R. Syversveen, K.-A. Lie, J. Tveranger, J. M. Nordbotten, Impact of top-surface morphology on CO2 storage capacity, Int. J. Greenh. Gas Control 11 (0) (2012) 221–235. doi:10.1016/j.ijggc.2012.08.012.

[17] A. R. Syversveen, H. M. Nilsen, K.-A. Lie, J. Tveranger, P. Abrahamsen, A study on how top-surface morphology influences the storage capacity of CO_2 in saline aquifers, in: P. Abrahamsen, R. Hauge, O. Kolbjørnsen (Eds.), Geostatistics Oslo 2012, Vol. 17 of Quantitative Geology and Geostatistics, Springer Netherlands, 2012, pp. 481–492. doi:10.1007/978-94-007-4153-9_39.

[18] V. Singh, A. Cavanagh, H. Hansen, B. Nazarian, M. Iding, P. Ringrose, Reservoir modeling of CO_2 plume behavior calibrated against monitoring data from Sleipner, Norway, in: SPE Annual Technical Conference and Exhibition, 19-22 September 2010, Florence, Italy, 2010, SPE 134891-MS. doi:10.2118/134891-MS.